

Balance Scene Learning Mechanism for Offshore and Inshore Ship Detection in SAR Images

Tianwen Zhang, Xiaoling Zhang, Jun Shi, Shunjun Wei, Jianguo Wang, Jianwei Li, Hao Su, and Yue Zhou

Abstract—Huge imbalance of different scenes’ sample numbers seriously declines Synthetic Aperture Radar (SAR) ship detection accuracy. Thus, to solve this problem, this letter proposes a novel Balance Scene Learning Mechanism (BSLM) for both offshore and inshore ship detection in SAR images. BSLM consists of three steps: 1) based on unsupervised representation learning, we establish a Generative Adversarial Network (GAN) to automatically extract SAR images’ scene features via the confrontation between a generator and a discriminator; 2) based on these features, we perform a SAR images’ scene binary cluster (offshore and inshore) using k -means algorithm; 3) based on the analysis of k -means cluster results, we augment the small cluster’s (inshore) sample number via simple sample replication to balance another big cluster’s (offshore) sample number, in order to eliminate different scenes’ learning bias and obtain balanced learning representation ability that can enhance learning benefits and improve detection accuracy. We apply BSLM to four widely-used and open-sourced detectors, i.e., Faster Regions-Convolutional Neural Network (Faster R-CNN), Cascade R-CNN, Single Shot multi-box Detector (SSD), and RetinaNet to confirm its effectiveness. Experimental result on the open SAR Ship Detection Dataset (SSDD) reveal that BSLM can greatly improve detection accuracy, especially for more complex inshore scenes.

Index Terms—Synthetic Aperture Radar (SAR), Ship Detection, Offshore, Inshore, Balance Scene Learning Mechanism (BSLM)

I. INTRODUCTION

SHIP detection in Synthetic Aperture Radar (SAR) images is attracting much attention from more and more scholars [1]-[26] due to its great value in traffic control, shipwreck rescue, fishery management, environmental monitoring, etc.

So far, some traditional SAR ship detection methods have been proposed [1]-[4]. For example, Hou *et al.* [1] proposed a multilayer Constant False Alarm Rate (CFAR) SAR ship detector. Zhu *et al.* [2] proposed a template-based SAR ship detection method. Xie *et al.* [3] and Zhai *et al.* [4] proposed saliency-based methods for inshore SAR ship detection. However, these traditional feature extraction methods have huge difficulty in detecting more complex inshore ships, shown in Fig. 1(b).

This work was supported in part by the National Natural Science Foundation of China under Grant 61571099, 61501098 and 61671113, and in part by the National Key R&D Program of China under Grant 2017YFB0502700. (Corresponding author: Xiaoling Zhang.)

T. Zhang, X. Zhang, J. Shi, S. Wei, J. Wang and H. Su are with the School of Information and Communication Engineering, University of Electronic Science and Technology of China, Chengdu 611731, China (e-mail: twzhang@std.uestc.edu.cn; xlzhang@uestc.edu.cn; shijun@uestc.edu.cn; weishunjun@uestc.edu.cn; wang_jg@uestc.edu.cn; suhao@std.uestc.edu.cn).

J. Li is with the 3rd Graduate Student Team, Naval Aeronautical University, Yantai 264000, China (e-mail: lgm_jw@163.com).

Y. Zhou is with the School of Electronic Information and Electrical Engineering, Shanghai Jiao Tong University, Shanghai 200240, China (e-mail: sjtu_zy@sjtu.edu.cn).

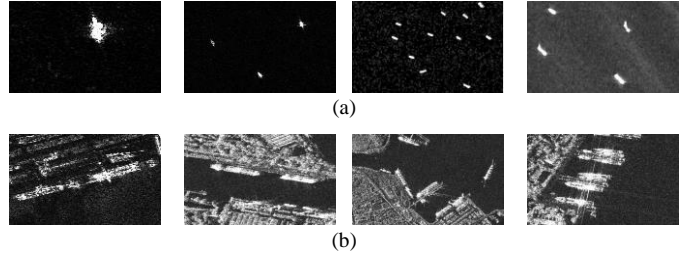


Fig. 1 Ships in SAR images. (a) Offshore scenes; (b) Inshore scenes.

Recent years, as the emergence of many deep learning object detectors, e.g., Faster R-CNN [5], Cascade R-CNN [6], SSD [7], RetinaNet [8], etc., increasing scholars [9]-[26] in the SAR community begin to devote themselves to deep learning-based SAR ship detectors. For example, 1) Based on Faster R-CNN, Cui *et al.* [9] proposed a dense attention pyramid network for multi-scale SAR ship detection. Lin *et al.* [10] proposed a squeeze and excitation Faster R-CNN to improve SAR ship detection performance. 2) Based on Cascade R-CNN, Wei *et al.* [11] proposed a high-resolution SAR ship detection network. Li *et al.* [12] proposed a cascade smoothing operator to ease speckle noise so as to improve detection accuracy. 3) Based on SSD, Wang *et al.* [13] studied transfer learning for SAR ship detection. Yang *et al.* [14] fused multi-scale feature on SSD to detect multi-scale ships. 4) Based on RetinaNet, Wang *et al.* [15] performed SAR ship detection in Gaofen-3 images. Liu *et al.* [16] proposed an improved loss function to enhance detection performance. However, the above modern deep learning methods pay less attention to more complex inshore scenes and still have poor accuracy for inshore scenes in Fig. 1(b).

In short, it is essential to study on both offshore and inshore SAR ship detection. Moreover, in our previous work [17]-[22], we found that the detection accuracy of complex inshore scenes is also too poor, seriously hindering our further progress. After our analysis and critical thinking, we hold the view that it is the huge imbalance of different scenes’ sample numbers that leads to the huge imbalance of learning representation ability. As a result, the detection accuracy of inshore scenes is far inferior to that of offshore scenes.

Thus, to solve this problem, this letter proposes a novel Balance Scene Learning Mechanism (BSLM) for both offshore and inshore SAR ship detection. BSLM consists of three steps: 1) using unsupervised representation learning, we establish a Generative Adversarial Network (GAN) [27] to automatically extract different scenes’ features in unsupervised via the internal learning confrontation between a generator and a discriminator; 2) using extracted features, we conduct a scene binary cluster of SAR images (inshore and offshore) by k -means algorithm, therinto, one cluster has less samples (inshore samples) and

another one has more samples (offshore samples); 3) based on clustering results, we augment the sample number of the small cluster via simple sample replication in order to balance the sample number of another big cluster, so as to eliminate different scenes' learning bias and achieve balanced learning representation ability of different scenes, which can enhance learning benefits and improve detection accuracy. To verify universal effectiveness of BSLM, we apply it to four widely-used and open-sourced detectors, i.e., two high-accurate but low-speed two-stage detectors (Faster R-CNN and Cascade R-CNN) and two high-speed but low-accurate one-stage detectors (SSD and RetinaNet). Experimental results on the open SAR Ship Detection Dataset (SSDD) [12] show that BSTM can greatly improve detection accuracy especially for more complex inshore scenes. Moreover, BSTM's accuracy gain is more remarkable for one-stage detectors that have biggest shortcomings of low-accuracy. Notably, BSLM is a universal mechanism that is also useful for other object detectors and other SAR datasets, of great value.

The main contributions of this letter are as follows:

- 1) BSLM is proposed to balance different scenes' learning representation ability for both offshore and inshore SAR ship detection.
- 2) GAN is used to automatically extract different scenes' features based on unsupervised representation learning.
- 3) BSLM can dramatically improve the detection accuracy of Faster R-CNN, Cascade R-CNN, SSD and RetinaNet.

II. METHODOLOGY

A. Motivation of BSLM

1) Motivation 1: Online Hard Example Mining

Shrivastava *et al.* [28] proposed Online Hard Example Mining (OHEM) to excavate hard samples. In OHEM, the samples with big training losses are regarded as hard ones that are accumulated to a sample pooling, and when the sample number in the pooling equals the training batch size, they will be put back networks to train again. In general, inshore samples can be seen as hard ones and the offshore as easy ones. However, OHEM is sensitive to noise labels [29] that widely exist in most SAR datasets, so it is not suitable for SAR ship detection (we have tried but got worse detection performance).

Therefore, it is essential to excavate inshore samples for emphatical training to enhance their learning representation ability.

2) Motivation 2: Balance Learning

Pang *et al.* [29] found three imbalance problems in object detection, i.e., positive-negative sample imbalance, feature imbalance and object imbalance. Moreover, we also found SAR images' scene imbalance problem, i.e., offshore samples often account for a bigger proportion than inshore ones in the whole data. This phenomenon is consistent with almost all existing SAR ship datasets, and also seems to accord with the fact that ocean area of the earth is much larger than land.

In general, more learning data can bring better learning effects. Therefore, SAR images' scene imbalance can lead to a big learning bias, i.e., detectors can obtain a strong learning representation for offshore scenes due to more offshore samples, but a poor one for inshore scenes due to less inshore samples.

As a result, leaving aside the differences in scene complexity, just considering the big gap in different scenes' sample numbers,

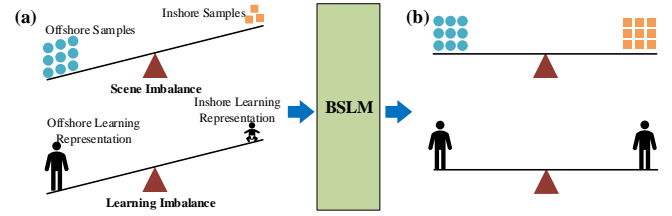


Fig. 2 Scene imbalance and learning imbalance.

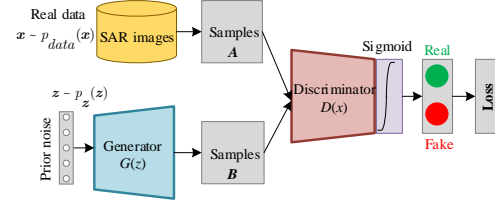


Fig. 3 Model of GAN.

the accuracy of the inshore inevitably is inferior to the offshore, for its poor learning representation ability. See Fig. 2(a).

Thus, it is essential to balance different scenes' sample numbers in order to achieve balanced scene learning representation. Finally, BSLM is proposed to make the above two imbalances in Fig. 2(a) to be balanced again. See Fig. 2(b).

B. Implementation of BSLM

1) Step 1: Scene Feature Extraction in Unsupervised

From Fig. 2, the most important core of BSLM is how to automatically distinguish samples of different scenes. In fact, this is a rather challenging task because we have no prior information about various SAR ship datasets. That is, in fact, we do not know whether images belong to inshore scenes or offshore scenes, because dataset's publishers did not provide real labels. Therefore, such scene feature extraction is an unsupervised process that is certainly our core work of this letter.

It is not advisable to use traditional methods to extract scene features due to limited generalization ability and too much human intervention. Fortunately, GAN [27], a most expected unsupervised algorithm [30], makes this problem solved smoothly.

So far, using unsupervised representation learning, Lin *et al.* [30] have applied GAN for the scene feature extraction of optical remote sensing images and Radford *et al.* [31] also have applied GAN for the scene feature extraction of natural images. Inspired by their work, we also adopt GAN to extract the features of different scenes, i.e., inshore scene and offshore scene.

a). Model of GAN

Fig. 3 shows the model of GAN. From Fig.3, a GAN consists of a generator $G(z)$ and a discriminator $D(x)$. The input of the generator $G(z)$ is a random prior noise z with a distribution $p_z(z)$ that is used to: 1) learn the generator's distribution p_g on the real data x ; 2) represent a mapping to data space as $G(z; \theta_g)$ where G is a differentiable function of a network with parameters θ_g . The output of the generator $G(z)$ is the generated samples B . The inputs of the discriminator $D(x)$ are both the samples from the real data x with a distribution $p_{data}(x)$ and the generated samples B of the generator. The output of the discriminator $D(x)$ is a single scalar $D(x; \theta_d)$ that is used to represent the probability that x came from real samples A rather than fake samples B , by using a sigmoid function defined by $y = 1/(1+e^{-x})$.

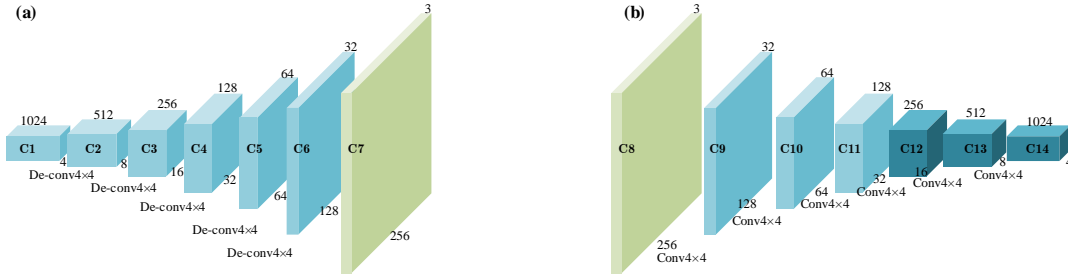


Fig. 4 Network architecture of Generative Adversarial Network (GAN). (a) Generator $G(z)$. (b) Discriminator $D(x)$.

In training, the generator $G(z)$ generates fake samples B that come from its learning on the real samples A meanwhile the discriminator $D(x)$ strives to distinguish fake samples B from real samples A . Then, based on the feedback of the training loss function, the generator $G(z)$ will learn harder to make fake samples B more and more close to real samples A , so as to deceive the discriminator $D(x)$. However, the discriminator $D(x)$ will also work harder to improve its identification ability so as to resist the cheating of the generator $G(z)$. Finally, the above confrontation process between the generator $G(z)$ and the discriminator $D(x)$ enables GANs to accurately learn the real data distribution [27].

b). Network Architecture of GAN

Same to Radford *et al.* [31], we establish the GAN, shown in Fig. 4. From Fig. 4, there are 7 deconvolutional blocks in the generator (C1~C7) and 7 convolutional blocks in the discriminator (C8~C14). The network input of the generator is set as a 100-dimension random noise vector obeying a uniform distribution. After a series of deconvolution operations, it is mapped into an output image with $256 \times 256 \times 3$ dimension. Then, the real samples A and generated samples B are inputted to the discriminator network. After a series of convolution operations, they are mapped into a feature vector with $1024 \times 4 \times 4$ dimension.

Same to Lin *et al.* [30], we concatenate the last 3 convolution blocks' feature maps (C12, C13 and C14) in the discriminator to form the scene feature vector of SAR images F , in order to aggregate the mid- and high-level information [30], i.e.,

$$F = \text{flatten} \left(F_{C14} \odot \text{MaxPool}^{2 \times} (F_{C13}) \odot \text{MaxPool}^{4 \times} (F_{C12}) \right) \quad (1)$$

where F_{C12} , F_{C13} and F_{C14} respectively denotes the feature maps of C12, C13 and C14, \odot denotes concatenate operation, $\text{MaxPool}^{2 \times}$ and $\text{MaxPool}^{4 \times}$ respectively denotes 2 times and 4 times max pooling, and flatten is used to reshape feature maps into a column vector, i.e., from $\mathbb{R}^{1792 \times 4 \times 4}$ to $\mathbb{R}^{28672 \times 1 \times 1}$ where 1792 equals $256+512+1024$ and 28672 equals $1792 \times 4 \times 4$. Finally, the scene feature vector of SAR images,

$$F = (f_1, f_2, f_3, \dots, f_{28671}, f_{28672})^T \quad (2)$$

is inputted to k -means algorithm for clustering analysis.

c). Training of GAN

When training $D(x)$, $G(z)$ is frozen, and equally, when training $G(z)$, $D(x)$ is frozen. We train D to maximize $D(G(z))$ that means assigning the correct label to real samples and samples from G . Similarly, we train G to minimize $\log[1-D(G(z))]$. Finally, D and G play the two-player minimax game with value function $V(G, D)$ [27]:

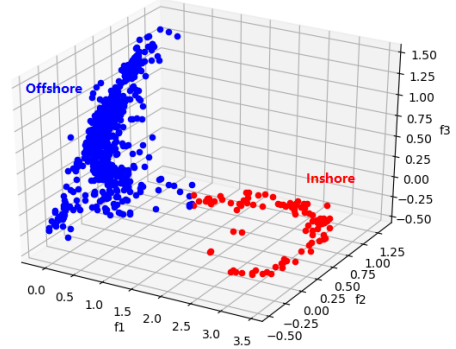


Fig. 5 Clustering results of k -means

$$\min_G \max_D V(D, G) = \mathbb{E}_{x \sim p_{\text{data}}(x)} [\log D(x)] + \mathbb{E}_{z \sim p_z(z)} [\log(1 - D(G(z)))] \quad (3)$$

More details about GAN can be found in [27], [30], [31].

2) Step 2: Scene Binary Cluster

Based on the scene feature vector of SAR images F , here, the k -means algorithm is used to conduct a binary cluster. Fig. 5 shows the clustering results of k -means on the training set of the SSDD dataset. To be clear, we only visualized (f_1, f_2, f_3) of Eq. (2) for more intuitive observation.

According to our observation, almost all inshore samples can be classed into the small cluster with less samples meanwhile almost all offshore samples can be classed into another big cluster. Thus, this fully shows that the scene features F extracted by GANs are rather effective to distinguish inshore scene and offshore scene, which avoids the heavy feature engineering of traditional methods. To be honest, we cannot do strict quantitative performance evaluation of clustering, because SSDD's publisher [12] did not provide the real labels of inshore or offshore.

Therefore, at last, we regard the cluster with less samples as inshore scene and that with more samples as offshore scene. In fact, our such practice is also certainly in line with the actual application situation, because, in almost all the existing SAR ship datasets, the number of inshore samples is universally less than that of offshore ones, which also seems to accord with the fact that ocean area of the earth is also much larger than land.

3) Step 3: Inshore Sample Augmentation

Finally, we augment the small cluster with less samples (inshore samples) by simple sample replication to make the sample number of two clusters basically equal so as to obtain a balance between the inshore and the offshore. Finally, the learning bias of different scenes is eliminated and the learning representation of different scenes is balanced, bringing better learning benefits.

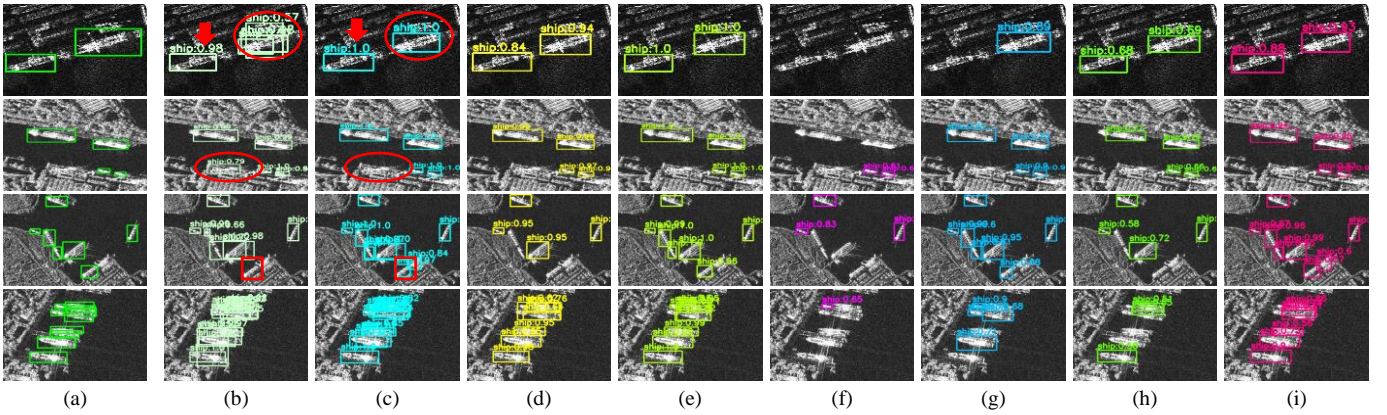


Fig. 6 SAR ship detection results. (a) Ground truth; (b) Faster R-CNN; (c) Faster R-CNN + BSLM; (d) Cascade R-CNN; (e) Cascade R-CNN + BSLM; (f) SSD; (g) SSD + BSLM; (h) RetinaNet; (i) RetinaNet + BSLM.

TABLE I
EVALUATION INDEXES OF DIFFERENT METHODS WITH BSLM OR WITHOUT BSLM

Type	Method	Inshore + Offshore			Inshore			Offshore		
		Recall	Precision	mAP	Recall	Precision	mAP	Recall	Precision	mAP
Two-stage	Faster R-CNN	89.34%	83.51%	88.26%	70.35%	62.05%	66.22%	98.12%	94.32%	97.68%
	Faster R-CNN + BSLM	92.10%	89.95%	91.13%	78.49%	77.14%	74.82%	98.39%	95.81%	98.18%
	Cascade R-CNN	88.97%	94.16%	88.67%	69.19%	83.80%	68.00%	98.12%	98.12%	98.00%
	Cascade R-CNN + BSLM	92.10%	92.95%	91.53%	78.49%	82.32%	76.32%	98.39%	97.60%	98.25%
One-stage	SSD	69.49%	96.43%	68.93%	47.67%	87.23%	46.52%	79.57%	99.33%	79.38%
	SSD + BSLM	78.12%	93.82%	76.59%	67.44%	85.29%	64.67%	83.06%	97.48%	82.44%
	RetinaNet	72.43%	94.26%	71.51%	48.26%	83.00%	45.66%	83.60%	97.80%	83.35%
	RetinaNet + BSLM	81.80%	84.28%	77.85%	68.02%	61.26%	58.06%	88.17%	97.33%	87.50%

III. EXPERIMENTS

A. Dataset

We use the first open SSDD dataset [12] to verify our work. There are 1160 images with 500×500 average size in SSDD¹ that are collected from Sentinel-1, TerraSAR-X and RadarSat-2 satellites. SAR images in SSDD have diversified polarizations, various resolutions and abundant ship scenes.

B. Training Details

In the MMDetection toolbox [32], we apply BSTM to four widely-used and open-sourced detectors, i.e., Faster R-CNN, Cascade R-CNN, RetinaNet and SSD. Among them, we use ResNet-50-FPN [29] as backbones of the first three and use VGG-16 as backbone of SSD. SAR images are resized into 512×512 [25] to input to networks. We train them for 12 epochs by Stochastic Gradient Descent (SGD) [32] optimization algorithm with learning rate = 0.02, momentum = 0.9 and weight decay = 0.001, on RTX2080Ti GPU of batch size 4 images.

C. Evaluation Indexes

Recall, Precision and mean Average Precision (mAP) are defined by:

$$\text{Recall} = \text{TP} / (\text{TP} + \text{FN}) \quad (4)$$

$$\text{Precision} = \text{TP} / (\text{TP} + \text{FP}) \quad (5)$$

$$\text{mAP} = \int_0^1 P(R) dR \quad (6)$$

¹In our previous work [17]-[22], the dataset is randomly divided into a training set, a validation set and a test set by 7:2:1 ratio, initially suggested by its publisher Jianwei Li [12], a co-author of this letter. However, for limited samples, random partition may bring serious accuracy randomness on the test set. Thus, Li *et al.* [12] appeal scholars of this field to use the 8:2 ratio as a training set and a test set (image indexes' suffix 1 and 9 as the test set). Moreover, we also revised the error labels of the test set and the revised test set is available on: https://pan.baidu.com/s/1YvsrP84l_At-svoZu44q-w (password: e5fn)

where TP is True Positive number, FN is False Negative number, FP is False Positive number, $P(R)$ is Precision-Recall curve and R is Recall.

IV. RESULTS

A. SAR Ship Detection Results

Fig. 6 shows the detection results of different methods. Intersection Over Union (IOU) [19] and score thresholds are set as 0.5. From Fig. 6, when BSLM is applied to these four detectors, the detection performance is universally improved. Specifically, some original false alarms are suppressed (marked in red ellipse) and some original missed detections are detected again (marked in red rectangle). Moreover, the confidence scores also universally become higher (marked in red arrow).

B. Quantitative Performance Comparison

Table I shows their evaluation indexes. Fig. 7 shows their $P(R)$ curves. From Table I, we can find that:

- 1) On the offshore and inshore scenes, BSLM respectively improved Faster R-CNN, Cascade R-CNN, SSD and RetinaNet by 2.87%, 2.86%, 7.66% and 6.34% mAP.
- 2) On the inshore scenes, BSLM respectively improved Faster R-CNN, Cascade R-CNN, SSD and RetinaNet by 8.60%, 8.32%, 18.15% and 12.40% mAP. Obviously, the learning representation of inshore scenes is greatly enhanced.
- 3) On the offshore scenes, BSLM respectively improved Faster R-CNN, Cascade R-CNN, SSD and RetinaNet by 0.50%, 0.25%, 3.06% and 4.15% mAP. Notably, while enhancing inshore learning ability, offshore one does not become weak but a litter stronger. One possible reason may be that without BSLM, networks may happen overfitting due to too many offshore samples' over-learning, causing modest generalization ability, but with BSLM, networks can distract partial attention to the inshore, avoiding the above over-learning.

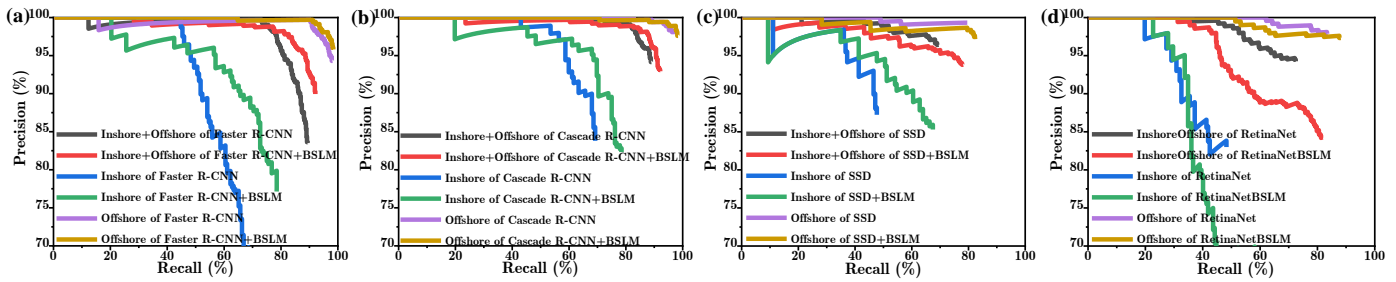


Fig. 7 P(R) curves. (a) Faster R-CNN and Faster R-CNN + BSLM; (b) Cascade R-CNN and Cascade R-CNN + BSLM; (c) SSD and SSD + BSLM; (d) RetinaNet and RetinaNet + BSLM.

- 4) The accuracy gap between inshore and offshore still exists, but their gap is far lower than the original one, showing BSLM's great function. However, given the inherent difference of scene complexity, it is unrealistic to make the accuracy of inshore and offshore fully equal. Our goal of this letter is to narrow such accuracy gap.

Finally, we also found that when BSLM is applied to one-stage detectors, its accuracy gain is more than two-stage ones, so it can solve existing most one-stage detectors' biggest defect of poor accuracy. To be clear, BSLM is used merely when training detectors, so it does not decline the detection speed.

V. CONCLUSIONS

Aiming at different scenes' sample imbalance, we propose a BSLM for multi-scene SAR ship detection. BSLM consists of three steps: 1) a GAN is used to extract scene features by unsupervised representation learning; 2) k -means is used to perform a scene binary cluster; 3) the sample number of the small cluster is augmented same as that of the big cluster. Finally, detectors eliminated different scenes learning bias. Experimental result on SSDD show that BSLM greatly improved detection accuracy of Faster R-CNN, Cascade R-CNN, SSD and RetinaNet. Notably, BSLM is a universal mechanism that is also effective for more other detectors and SAR datasets. Given limited pages, we do not show their results any more in this letter.

Our work in this letter is of great meaning, because:

- 1) We innovatively solved different scenes' detection imbalance from the point of view of datasets themselves, even though simple but rather effective. This balance idea is very significant that is also applicable to other more datasets in other more detection tasks.
- 2) We originally used GAN to extract SAR images' scene features in unsupervised, and identified offshore or inshore by k -means, providing a new future study idea, e.g., network scene adaption, detection after scene classification, etc.

REFERENCES

- [1]. B. Hou, *et al.*, "Multilayer CFAR detection of ship targets in very high-resolution SAR images," *IEEE Geosci. Remote Sens. Lett.*, vol. 12, no. 4, pp. 811-815, 2015.
- [2]. J. Zhu, *et al.*, "Projection shape template-based ship target recognition in TerraSAR-X images," *IEEE Geosci. Remote Sens. Lett.*, vol. 14, no. 2, pp. 222-226, 2017.
- [3]. T. Xie, *et al.*, "Inshore ship detection based on level set method and visual saliency for SAR Images," *Sensors*, vol. 18, no. 11, pp. 3877, 2018.
- [4]. L. Zhai, *et al.*, "Inshore ship detection via saliency and context information in high-resolution SAR images," *IEEE Geosci. Remote Sens. Lett.*, vol. 13, no. 12, pp. 1870-1874, 2016.
- [5]. S. Ren, *et al.*, "Faster R-CNN: Towards real-time object detection with region proposal networks," *arXiv:1506.01497*.
- [6]. Z. Cai, *et al.*, "Cascade R-CNN: Delving into high quality object detection," *arXiv:1712.00726*.
- [7]. W. Liu, *et al.*, "SSD: Single shot multibox detector," *arXiv:1512.02325*.
- [8]. T. Lin, *et al.*, "Focal loss for dense object detection," *arXiv:1708.02002*.
- [9]. Z. Cui, *et al.*, "Dense attention pyramid networks for multi-scale ship detection in SAR images," *IEEE Trans. Geosci. Remote Sens.*, vol. 57, no. 11, pp. 8983-8997, 2019.
- [10]. Z. Lin, *et al.*, "Squeeze and excitation rank Faster R-CNN for ship detection in SAR images," *IEEE Geosci. Remote Sens. Lett.*, vol. 16, no. 5, pp. 7, 2019.
- [11]. S. Wei, *et al.*, "Precise and robust ship detection for high-resolution SAR imagery based on HR-SDNet," *Remote Sens.*, vol. 12, no. 167, 2020.
- [12]. J. Li, *et al.*, "A ship detection method based on Cascade CNN in SAR images," *Control Decision*, vol. 34, no. 10, pp. 2191-2197, 2019.
- [13]. Y. Wang, *et al.*, "Combining a single shot multibox detector with transfer learning for ship detection using Sentinel-1 SAR images," *Remote Sens. Lett.*, vol. 9, no. 8, pp. 780-788, 2018.
- [14]. L. Yang, *et al.*, "SAR ship detection based on convolutional neural network with deep multiscale feature fusion," *Acta Optica Sinica*, vol. 40, no. 2, pp. 215, 2020.
- [15]. Y. Wang, *et al.*, "Automatic ship detection based on RetinaNet using multi-resolution Gaofen-3 imagery," *Remote Sens.*, vol. 11, no. 5, pp. 531, 2019.
- [16]. J. Liu, *et al.*, "Ship target detection in SAR image based on RetinaNet," *J. Hunan. Univ. Nat. Sci.*, vol. 47, no. 2, pp. 85-91, 2020.
- [17]. T. Zhang, *et al.*, "HyperLi-Net: A hyper-light deep learning network for high-accurate and high-speed ship detection from synthetic aperture radar imagery," *ISPRS J. Photogramm. Remote Sens.*, early access, 2020.
- [18]. T. Zhang, *et al.*, "ShipDeNet-20: An only 20 convolution layers and <1 MB light-weight SAR ship detector," *IEEE Geosci. Remote Sens. Lett.*, early access, 2020.
- [19]. T. Zhang, *et al.*, "Depthwise separable convolution neural network for high-speed SAR ship detection," *Remote Sens.*, vol. 11, no. 2483, 2019.
- [20]. T. Zhang, *et al.*, "High-speed ship detection in SAR images based on a grid convolutional neural network," *Remote Sens.*, vol. 11, no. 120, 2019.
- [21]. X. Zhang, *et al.*, "High-speed and high-accurate SAR ship detection based on a depthwise separable convolution neural network," *J. Radars*, vol. 8, no. 6, pp. 841-851, 2019.
- [22]. T. Zhang, *et al.*, "High-speed ship detection in SAR images by improved yolov3," in *Proc. Int. Comput. Conf. Wavelet Active Med. Tech. and Inf. Process. (ICCWAMTIP)*, Chengdu, China, pp. 149-152, 2019.
- [23]. J. Zhao, *et al.*, "A coupled convolutional neural network for small and densely clustered ship detection in SAR images," *Sci. China Inf. Sci.*, vol. 62, no. 4, pp. 42301, 2018.
- [24]. Y. Zhao, *et al.*, "Attention Receptive Pyramid Network for Ship Detection in SAR Images," *IEEE J. Sel. Topics Appl. Earth Observ. Remote Sens.*, early access, 2020.
- [25]. Y. Mao *et al.*, "Efficient low-cost ship detection for SAR imagery based on simplified U-Net," *IEEE Access*, vol. 8, no. pp. 69742-69753, 2020.
- [26]. Z. Deng, *et al.*, "Learning deep ship detector in SAR images from scratch," *IEEE Trans. Geosci. Remote Sens.*, vol. 57, no. 6, pp. 4021-4039, 2019.
- [27]. I. G., *et al.*, "Generative adversarial networks," *arXiv:1406.2661*.
- [28]. A. Shrivastava, *et al.*, "Training region-based object detectors with online hard example mining," *arXiv:1604.03540*.
- [29]. J. Pang, *et al.*, "Libra R-CNN: Towards balanced learning for object detection," *arXiv:1904.02701*.
- [30]. D. Lin, *et al.*, "MARTA GANs: unsupervised representation learning for remote sensing image classification," *IEEE Geosci. Remote Sens. Lett.*, vol. 14, no. 11, pp. 2092-2096, 2017.
- [31]. A. Radford, *et al.*, "Unsupervised representation learning with deep convolutional generative adversarial networks," *arXiv:1511.06434*.
- [32]. MMDetection. Available: <https://github.com/open-mmlab/mmdetection>